analytical chemistry

Article

pubs.acs.org/ac

Principal Component Analysis (PCA)-Assisted Time-of-Flight Secondary-Ion Mass Spectrometry (ToF-SIMS): A Versatile Method for the Investigation of Self-Assembled Monolayers and Multilayers as Precursors for the Bottom-Up Approach of Nanoscaled Devices

Markus Holzweber,*[,†] Thomas Heinrich,[‡] Valentin Kunz,[‡] Sebastian Richter,[‡] Christoph H.-H. Traulsen,[‡] Christoph A. Schalley,[‡] and Wolfgang E. S. Unger[†]

[†]BAM—Bundesanstalt für Materialforschung und-prüfung, Unter den Eichen 44-46, 12203 Berlin, Germany

[‡]Institut für Chemie und Biochemie, Freie Universität Berlin, Takustraße 3, 14195 Berlin, Germany

ABSTRACT: The production of high-quality self-assembled monolayers (SAMs) followed by layer-by-layer (LbL) self-assembly of macrocycles is essential for nanotechnology applications based on functional surface films. To help interpret the large amount of data generated by a standard ToF-SIMS measurement, principal component analysis (PCA) was used. For two examples, the advantages of a combination of ToF-SIMS and PCA for quality control and for the optimization of layer-by-layer self-assembly are shown. The first example investigates how different cleaning methods influence the quality of SAM template formation. The second example focuses on the LbL self-assembly of macrocycles and the corresponding stepwise surface modification.

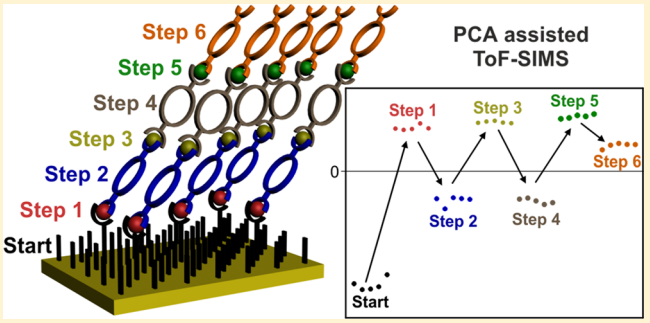

One objective of modern nanotechnology is the miniaturization of devices with function in order to increase performance while improving energy efficiency. In this context, the top-down approach has been applied extensively by researchers, as well as by producers. However, the bottom-up approach gained more attention in the last years, since it is easy to manage on a laboratory scale.[1,2] We have recently demonstrated the deposition of Hunter/Vögtle-type tetralactam macrocycles, amide rotaxanes, and gold nanoparticles into ordered and programmable monolayers and multilayers on gold substrates, using the metal-ion-mediated layer-by-layer (LbL) approach.[1,3,4] These surface films can be regarded as precursors of nanoscaled devices that may translate molecular stimuli into macroscopic effects.[5]

Because of the complexity of these systems, with regard to elemental composition, distribution, binding state, order, topology, or layer sequence, a major task is the choice and execution of suitable analytical techniques such as X-ray photoelectron spectroscopy (XPS), UV/vis spectroscopy, IR spectroscopy, and atomic force microscopy (AFM). Often, more-sophisticated techniques such as time-of-flight secondary-ion mass spectrometry (ToF-SIMS) are required, which provide excellent surface sensitivity on the molecular level combined with the possibility of depth-profiling and imaging.[6]

Recently, this has been demonstrated for self-assembled monolayers (SAMs) with terminal functional groups, such as pyridine or terpyridine, that are suitable for complex formation with transition-metal ions enabling subsequent deposition of monolayers and multilayers composed of macrocycles and rotaxanes.[7,8]

To produce high-quality layer systems, process control of the chemical surface modification is necessary. This can be achieved via ToF-SIMS which is a highly sensitive surface characterization technique that provides elemental and molecular surface chemical information. It has been shown that, in well-ordered SAMs, the organic molecule is in an upright conformation, thus having its functional group at the very surface.[9] For the present study, we anticipate the ToF-SIMS spectra to be very similar, as the tail is always (ter)-pyridine-terminated. Therefore, a univariate interpretation of the mass spectra is unreasonable and

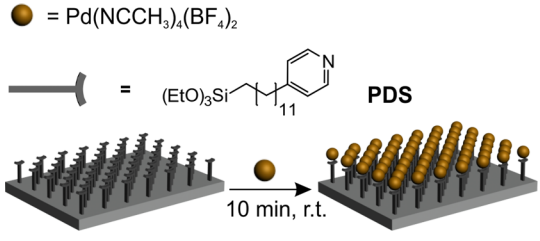

Figure 1. Idealized schematic depiction of the investigated template layer.

Received: January 6, 2014
Accepted: May 15, 2014
Published: May 15, 2014

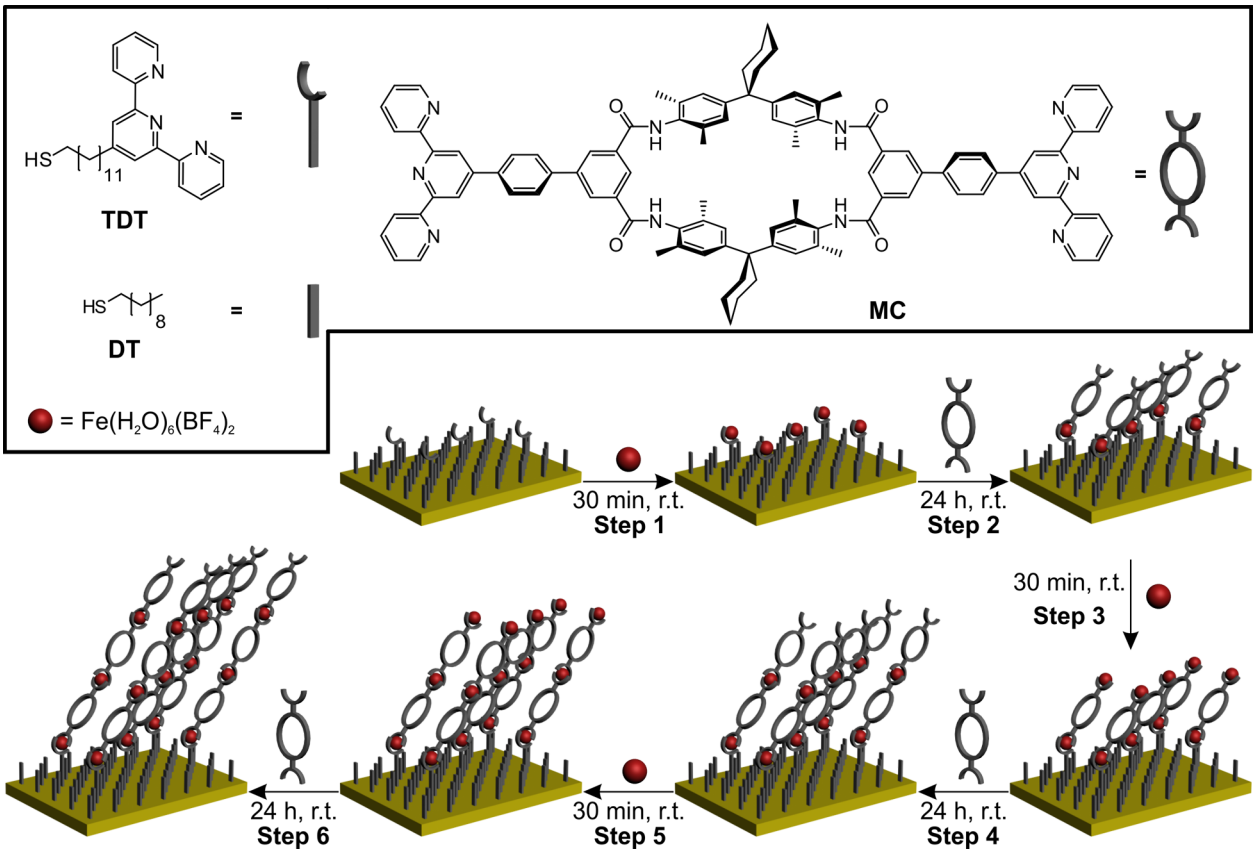

Figure 2. Idealized schematic depiction of the iron-mediated LbL self-assembly of **MC**. The underlying mixed SAM consists of a 1:3 mixture of **TDT** and **DT** molecules. In steps 1, 3, and 5, the sample is immersed in $Fe(H_2O)_6(BF_4)_2$ in ethanol (1 mM) for 30 min; in steps 2, 4, and 6, the sample is immersed in a solution of **MC** in dimethylformamide (DMF) (1 mM) for 24 h.

a multivariate approach has been chosen using principal component analysis (PCA). PCA is a multivariate statistical analysis method that can identify the major directions of variation in a given dataset. A dataset is defined as a matrix where the rows contain samples and columns contain variables. In the case of ToF-SIMS data, samples are the mass spectra and the variables are the individual m/z ratios. The PCA is calculated from the covariance matrix of this original data set. PCA is an axis rotation that aligns a new set of axes, called principal components (PCs) with the maximal directions of variance within a dataset. PCA creates three new matrices, containing the scores, the loadings, and the residuals.[10] Therefore, it aids in the interpretation of complex mass spectra (as is the case for organic ToF-SIMS spectra) by revealing differences between (groups of) *samples* (expressed as so-called "scores") and relating them back to differences in the *variables* (called "loadings") defining a sample.[11] The scores plot shows whether samples or a group of samples are different. The corresponding loadings plot shows the difference in the mass spectra and fragmentation pattern of the samples (or the group of samples).[10] In principle, PCA provides the ability to identify key fragment peaks characterizing a given sample type, a survey of the point-to-point reproducibility across the sample set, and a summary of the relationship between different sample sets.[12−15]

Here, we present the investigation of two examples by applying PCA-assisted ToF-SIMS. First, the cleaning procedure prior to the formation of a template SAM with a pyridyl-functional group and an aliphatic backbone on native silicon oxide is examined in detail. In order to find a suitable method, three different cleaning

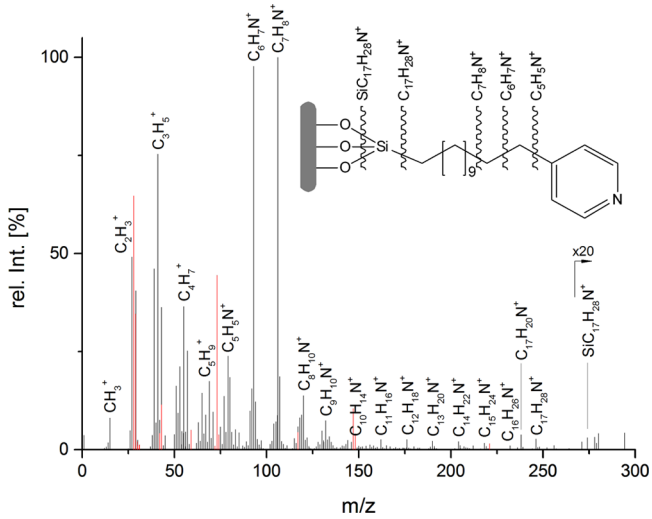

Figure 3. Positive-ion-mode ToF-SIMS spectrum of the **PDS** SAM. Peaks in red correspond to PDMS residues from the preparation procedure.

procedures are compared to each other, with respect to PC separation and detected contaminants. The used template layer is depicted in Figure 1 and is supposed to serve as a model for other functional template layers. The deposition of palladium(II) ions onto the SAM is also displayed.

In the second example, a much more complex system is investigated. A mixed template layer consisting of decanethiol (**DT**) and terpyridine-terminated dodecanethiol (**TDT**) in a ratio of

dx.doi.org/10.1021/ac500059a | *Anal. Chem.* 2014, 86, 5740−5748

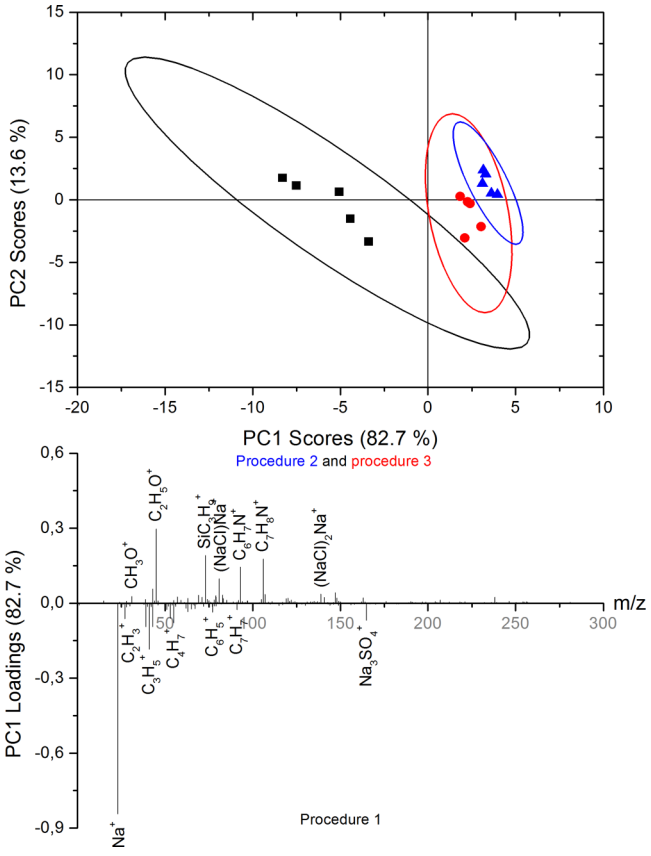

Figure 4. Scores plot of the first two principal components for the three different cleaning procedures (left) and the corresponding loadings plot showing the variables responsible for the separation on PC1. The percentage in the brackets denotes how much variance is caught by the corresponding principal component. [Legend: black squares, procedure 1; blue triangles, procedure 2; and red circles, procedure 3.] The ellipses show the 95% confidence limit.

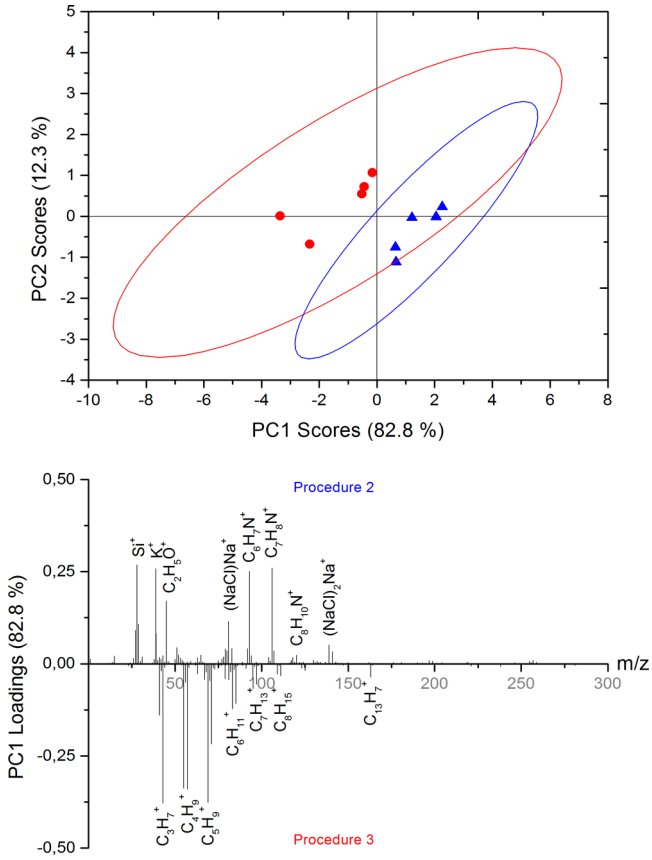

Figure 5. Score plot of the first two principal components for cleaning procedures 2 and 3 (left). The ellipses show the 95% confidence limit. The corresponding loadings plot of the first principal component shows the variables (m/z values) responsible for the separation on PC1. [Legend: blue triangles, procedure 2; red circles, procedure 3.]

3:1 on gold is used as a preordering template for a further deposition of macrocycles. In alternating steps, a layer of coordinating Fe(II) using $Fe(BF_4)_2 \cdot 6H_2O$ and a bis-terpyridine functionalized tetralactam macrocycle (**MC**) is deposited by LbL self-assembly (see scheme in Figure 2).

EXPERIMENTAL SECTION

Sample Preparation. Silicon wafers with thin oxide layers were activated by immersing them for 30 min in piranha solution ($H_2O_2/H_2SO_4 = 1/3$) and they were vigorously rinsed afterward with deionized water for 30 s or 2 min, immersed in Millipore water and ethanol, followed by dichloromethane. *[WARNING! Piranha solution must be handled with the utmost caution because it reacts violently with organic material.]* Pyridyldodecane silane (**PDS**) monolayers were prepared by immersing the activated substrates into a 5 mM solution of **PDS** in dichloromethane for 24 h at room temperature (rt). Palladium deposition on **PDS**-SAMs was performed by immersing the surfaces at rt for 10 min in a 1 mM solution of tetrakis(acetonitrile)palladium(II) tetrafluoroborate in acetonitrile.

Polycrystalline Au substrates were cleaned in concentrated HCl for 10 min and, afterward, were vigorously rinsed with deionized (DI) water and immersed in EtOH. Mixed monolayers were prepared by immersing the substrates into a 1 mM ethanolic solution of a 1:3 mixture of 12-(-(2,2′:6′,2″-terpyridine-4′-yl)-dodecane-1-thiol (**TDT**) and decane-1-thiol (**DT**) for 24 h at rt. Metal deposition was performed within 30 min at rt by immersing the SAMs into a 1 mM solution of iron(II) tetrafluoroborate hexahydrate in EtOH. Macrocycle (**MC**) deposition was carried out by immersing the surfaces into a 1 mM solution of **MC** in DMF. After finishing each deposition step, the samples were thoroughly washed with ethanol or dimethylformamide for 10 min, dried in a stream of argon, and stored under argon before characterization.

Time-of-Flight Secondary-Ion Mass Spectrometry (ToF-SIMS). All sample measurements were performed without further pretreatment on a ToF.SIMS IV instrument (ION-TOF GmbH, Münster, Germany) of the reflectron-type, equipped with a 25keV bismuth liquid metal ion gun (LMIG) as the primary ion source mounted at an angle of 45°, with respect to the sample surface. The LMIG was operated at 0.5 μA emission current in the so-called "high current bunched" mode (high mass resolution, low lateral resolution). Bi_3^+ was selected as primary ion by appropriate mass filter settings. To improve the focus of the primary ion beam, the pulse width of the Bi_3^+ (25 keV) ion pulse was reduced to 11 ns and the lens target was adjusted to obtain a sharp image on a structured sample (e.g., silver cross) in the secondary electron mode. The primary ion current was directly determined using a Faraday cup located on a grounded sample holder. Operation conditions with these settings comprised a target current of 0.15−0.17 pA for the selected primary ion. The total primary ion dose density was set to 5×10^{11} ions/cm^2, ensuring static conditions. Scanning area for analysis was

dx.doi.org/10.1021/ac500059a | Anal. Chem. 2014, 86, 5740−5748

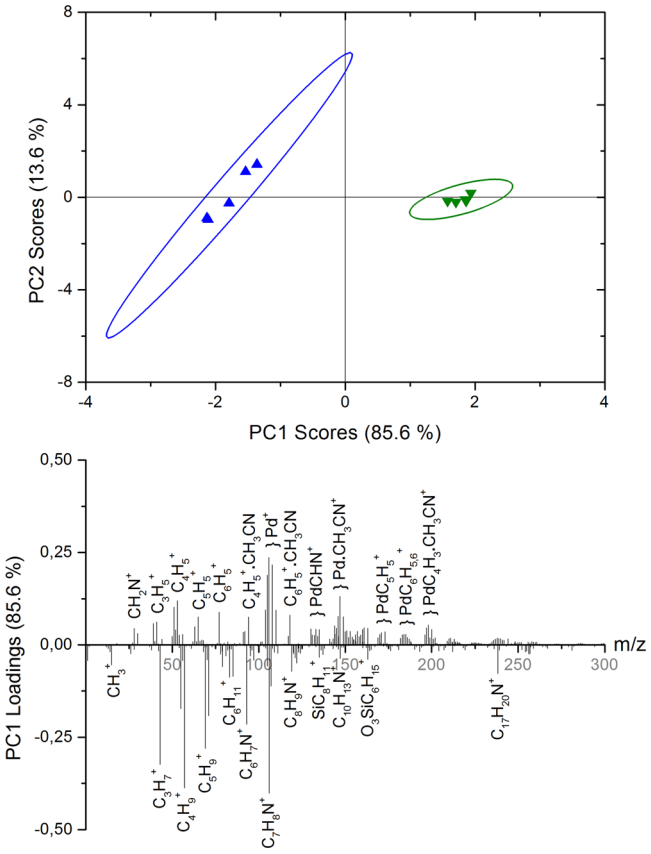

Figure 6. Scores plot of the first two principal components for the surface modification of the **PDS** SAM with $Pd(CH_3CN)_4(BF_4)_2$ as depicted in Figure 1. The ellipses show the 95% confidence limit. Corresponding loadings plot from the first principal component showing the variables responsible for the separation on PC1.

Table 1. Assignments of the Sample Numbers to Their Corresponding Surface-Modification Step

sample numbers	sample notation	modification step	
1–5	**TDT/DT**	Start	SAM template
6–10	**TDT/DT**-Fe	Step 1	Fe^{2+} coord. to SAM template
11–15	**TDT/DT**-Fe**MC**	Step 2	**MC** coord. to step 1
16–20	**TDT/DT**-Fe**MC**-Fe	Step 3	Fe^{2+} coord. to step 2
21–25	**TDT/DT**-(Fe**MC**)$_2$	Step 4	**MC** coord. to step 3
26–30	**TDT/DT**-(Fe**MC**)$_2$-Fe	Step 5	Fe^{2+} coord. to step 4
31–35	**TDT/DT**-(Fe**MC**)$_3$	Step 6	**MC** coord. to step 5

200 μm × 200 μm with a pixel resolution of 256 × 256. The vacuum in the analysis chamber was in the range of 10^{-9} mbar during all measurements.

ToF-SIMS spectra were acquired in positive-ion mode with five spots per sample analyzed. The mass scale was internally calibrated using several well-defined and easily assignable secondary ions. For the cleaning study (example 1) including a subsequent coordination of Pd^{2+} (see scheme in Figure 1) $C_4H_9^+$, $C_5H_{11}^+$, and $C_6H_{13}^+$ were used for the mass calibration. For the LbL self-assembly experiment (example 2), $C_3H_2^+$, $C_4H_2^+$, $C_5H_2^+$, and Au_3^+ were taken. The error in calibration (i.e., the error for those fragments solely used to calibrate the spectra)

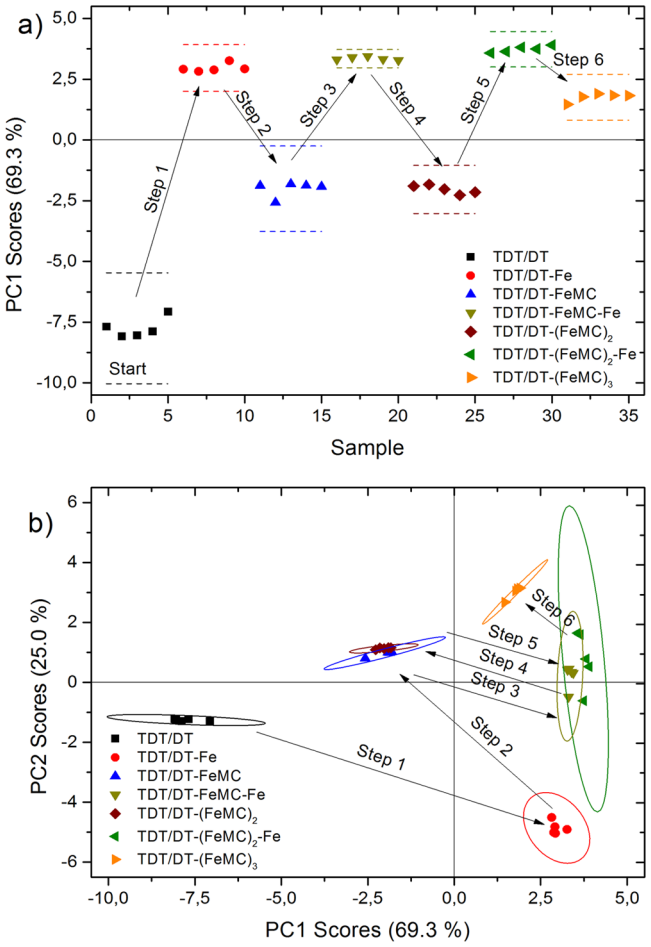

Figure 7. PCA scores plot of the entire dataset: (a) PC1 scores versus the sample number and (b) PC1 versus PC2 scores. The dashed lines in panel (a) and the ellipses in panel (b) denote the 95% confidence limit.

was kept below 10 ppm. The individual mass deviation of fragments not used for calibration might be larger. This level of calibration is required for a successful PCA and guarantees minimum scattering in peak positions and minimized errors in setting the integration limits. The approach outlined here ensures that the variance in the given dataset is due to real sample differences. Integration limits in m/z regions with overlapping peaks were placed tightly around each peak, to ensure consistent and accurate measurements of all peak areas.

Principal Component Analysis (PCA). The peak list creation strategy to perform PCA was carried out by selecting over 400 peaks in the mass range of m/z 0–350 for both, the survey of the cleaning procedure, including the subsequent coordination of Pd^{2+}, and the process control of the chemical surface modification by LbL self-assembly. PCA was performed using the software R version 2.15.2. [Here, R is an open access program for statistical computing, downloadable from http://www.r-project.org.] Each peak was normalized to the sum of the selected peak intensities to correct for variations in the total secondary ion yields between different spectra. The data were then mean-centered.[11]

RESULTS AND DISCUSSION

Example 1: Assessment of Cleaning Procedures for SAM Templates Including a Subsequent Coordination of Pd^{2+} to an Optimized SAM. In this study, a pyridyldodecane silane (**PDS**) SAM on hydroxyl-terminated silicon is generated

dx.doi.org/10.1021/ac500059a | Anal. Chem. 2014, 86, 5740–5748

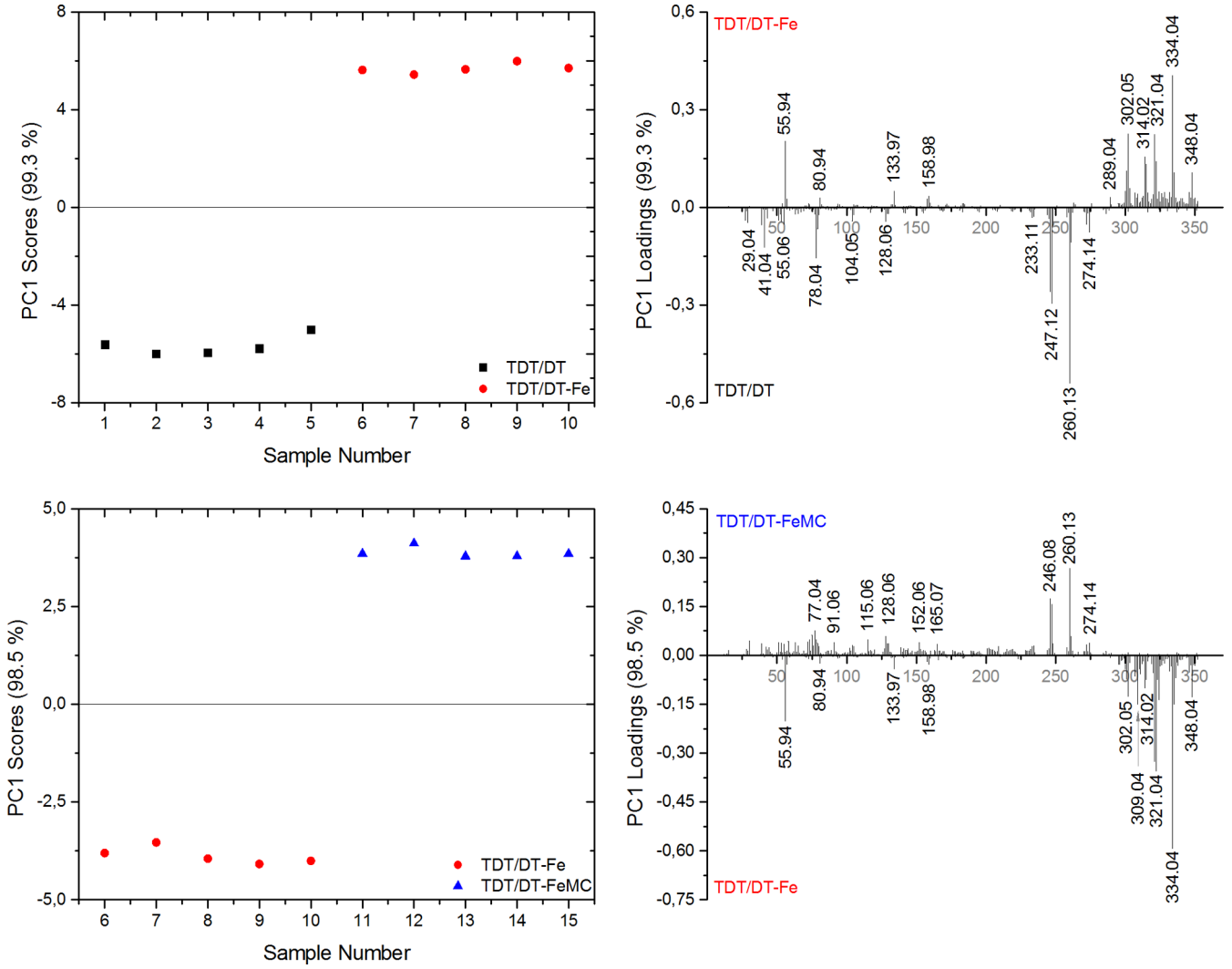

Figure 8. Scores and loadings plot for surface modification step 1 (top) and step 2 (bottom).

as a preordering template for a further coordinative LbL deposition. In the subsequent step, a layer of coordinating Pd(II), using $Pd(CH_3CN)_4(BF_4)_2$, is deposited.

Figure 3 shows the **PDS**-SAM and the corresponding ToF-SIMS mass spectrum obtained in positive-ion mode in the mass range from m/z 0 to 300. Since this mass spectrometric method is also very sensitive to contaminants on the surface, secondary ion signals from inorganic contaminations were removed from the spectrum in Figure 3 for clarification. Residues from polydimethylsiloxane (PDMS) are marked in red to show the relative intensities, compared to the SAM. [Here, PDMS is a ubiquitous contamination compound, primarily derived from ground joint grease used for the sealing and lubrication of ground glass joints during synthesis and workup.] The low mass range (up to m/z 75) shows hydrocarbon fragments originating from the dodecane alkyl spacer as well as low intensity mass fragments containing C, H and N originating from a cleavage of the pyridine tail group. The high mass range (m/z 75 to 250) shows secondary ion fragments with the typical fragmentation pattern (successive cleavage of CH_2) from the **PDS** precursor down to the intact pyridine tail group $C_5H_5N^+$ at m/z = 79.04. Although the **PDS** mother ion $SiC_{17}H_{28}N^+$ could be detected, its secondary ion yield is very low, compared to analogous thiol-based SAMs on Au.[16] This is most likely due to a much stronger binding of the silane headgroup to the silicon surface than thiol to a gold surface. Therefore, the $C_{17}H_{28}N^+$ secondary ion at m/z = 246.21 is a characteristic fragment taken as a proof of the formation of the **PDS**-SAM. This fragmentation pattern is consistent with that previously reported for the 12-(pyridine-4-yl)dodecane-1-thiol (PDT) on gold.[16]

In the initial experiments, a considerable contamination of sodium sulfate was observed after SAM formation. To reduce the contamination and, hence, enhance the quality of the SAM, different cleaning procedures prior to SAM formation were investigated using PCA. In the standard cleaning, we carried out a 30-s rinsing with deionized water (procedure 1). After finding the above-mentioned sulfate-impurities, we extended the rinsing process to 2 min in deionized water (procedure 2). Procedure 3 was composed of rinsing the surface for 2 min in deionized water, followed by a 10 min immersion in Millipore water after activation of the surface.

Figure 4 shows the score plot from a PCA of the positive secondary ions of the **PDS**-SAM by three different cleaning methods, which differ by the amount of time the surfaces are rinsed with deionized water. It can be seen that procedure 1 is clearly separated on PC1 from the other two procedures. The large scatter of the data shows a poor point-to-point reproducibility and the corresponding negative loadings reveal

dx.doi.org/10.1021/ac500059a | Anal. Chem. 2014, 86, 5740−5748

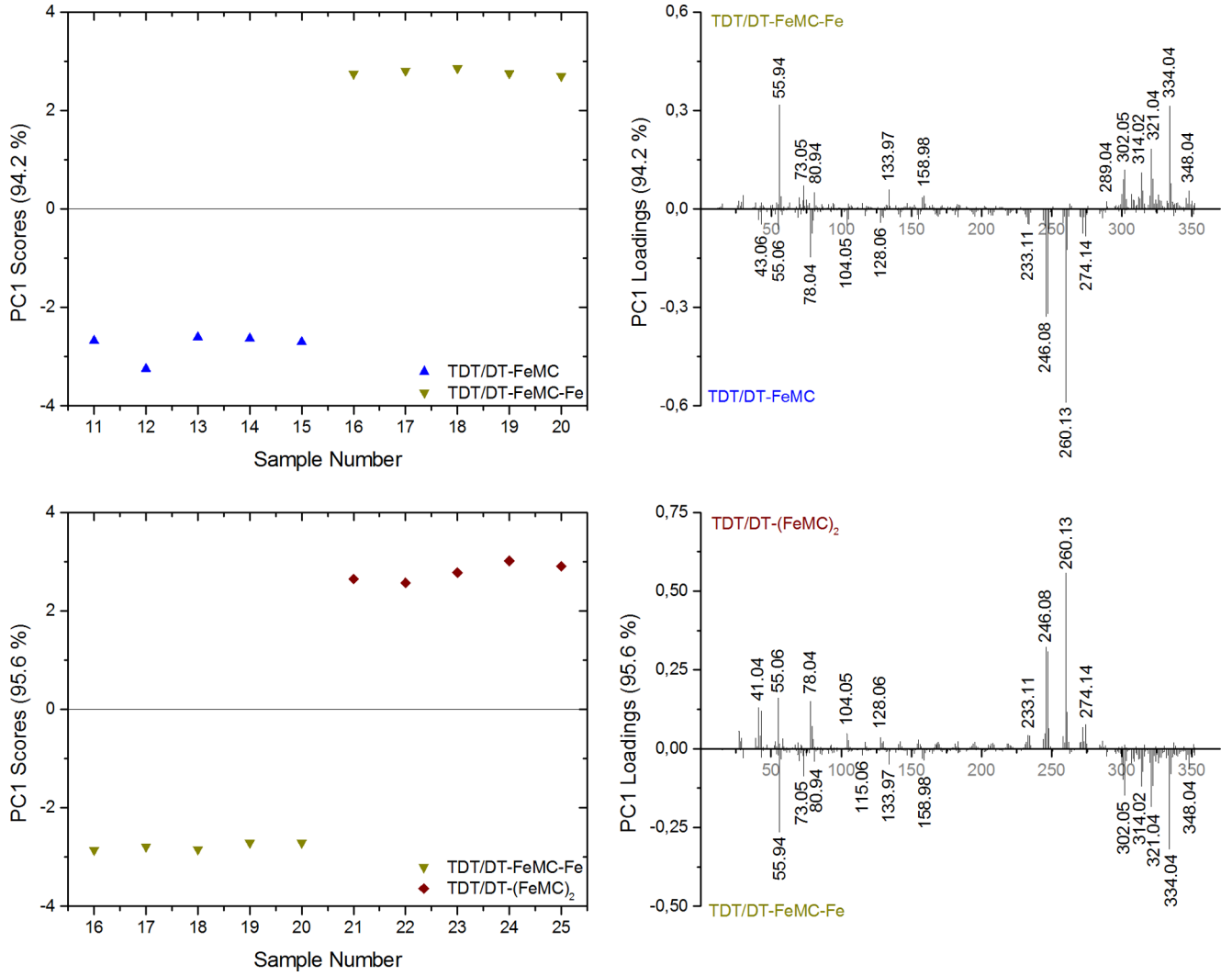

Figure 9. Scores and loadings plot for surface modification step 3 (top) and step 4 (bottom).

significant contamination of sodium sulfate by highlighting Na^+ and $Na_3SO_4^+$ secondary ions after PCA originating from the activation with piranha solution (sulfuric acid), demonstrating that not all acid was removed prior to SAM formation. This illustrates a contamination-caused inhomogeneity of the formed SAM. Some other generic contaminants, PDMS (Si^+ and $SiC_3H_9^+$ fragments) and sodium chloride (characteristic fragments) also have been observed. However, the positive loadings highlight secondary fragment ions that are characteristic for the formed **PDS** SAM (i.e., $C_6H_7N^+$ and $C_7H_8N^+$). It has been indicated by other authors that, if a SAM is packed more regularly and well-ordered, more molecular secondary ions characteristic for the SAM are emitted by the impact of a primary ion.[13,17] This holds true also for our SAMs prepared following the cleaning procedures 2 and 3. This result indicates a major advantage of procedures 2 and 3.

To distinguish cleaning procedure 2 from procedure 3, a PCA was carried out with only the two corresponding datasets (see Figure 5). The slight separation seen on PC2 in Figure 4 is now on PC1, and the variables responsible for the difference can be seen on the loadings plot in Figure 5. Note that the secondary fragment ions $C_2H_5O^+$ (at m/z = 45.03), $C_6H_7N^{\bullet\,+}$ (at m/z = 93.05), and $C_7H_8N^+$ (at m/z = 106.06), characterizing a well-ordered **PDS**-SAM, are more pronounced in the loadings plots in Figures 4 and 5 as the cleaning procedure improves, whereas Na^+ and hydrocarbon fragments are the major peaks in the negative loadings plot for cleaning procedure 1 (see Figure 4) and only the hydrocarbon fragments in cleaning procedure 3 (see Figure 5). Following the above conclusion for well-ordered SAMs, a more closely packed SAM is achieved after applying cleaning procedure 2. In addition, the preferential orientation of the SAM has been proven by the linear dichroism effect observed by angle-resolved near-edge X-ray absorption fine structure (NEXAFS) experiments.[1] Note that the additional rinsing with Millipore water in cleaning procedure 3 did not improve the quality of the SAM, although the opposite was expected. The overlapping 95% confidence limits in Figure 5 support this observation.

The fragment ions CH_3O^+ and $C_2H_5O^+$ are prominent in the loadings plot of Figure 4 but are not characteristic for a perfect SAM. Two possible origins of these ions can be considered: (i) ethanol is formed as a byproduct during the self-assembly of the triethoxysilyl precursor and (ii) these fragment ions originate from an uncompleted reaction of the triethoxysilyl precursor, i.e., not all three ethoxysilyl groups reacted with the silicon substrate or cross-linked among each other. Because of the extremely low pressure in the analysis chamber (10^{-9} mbar), assumption (i) is not likely, because all high-vapor pressure residues should be

dx.doi.org/10.1021/ac500059a | Anal. Chem. 2014, 86, 5740−5748

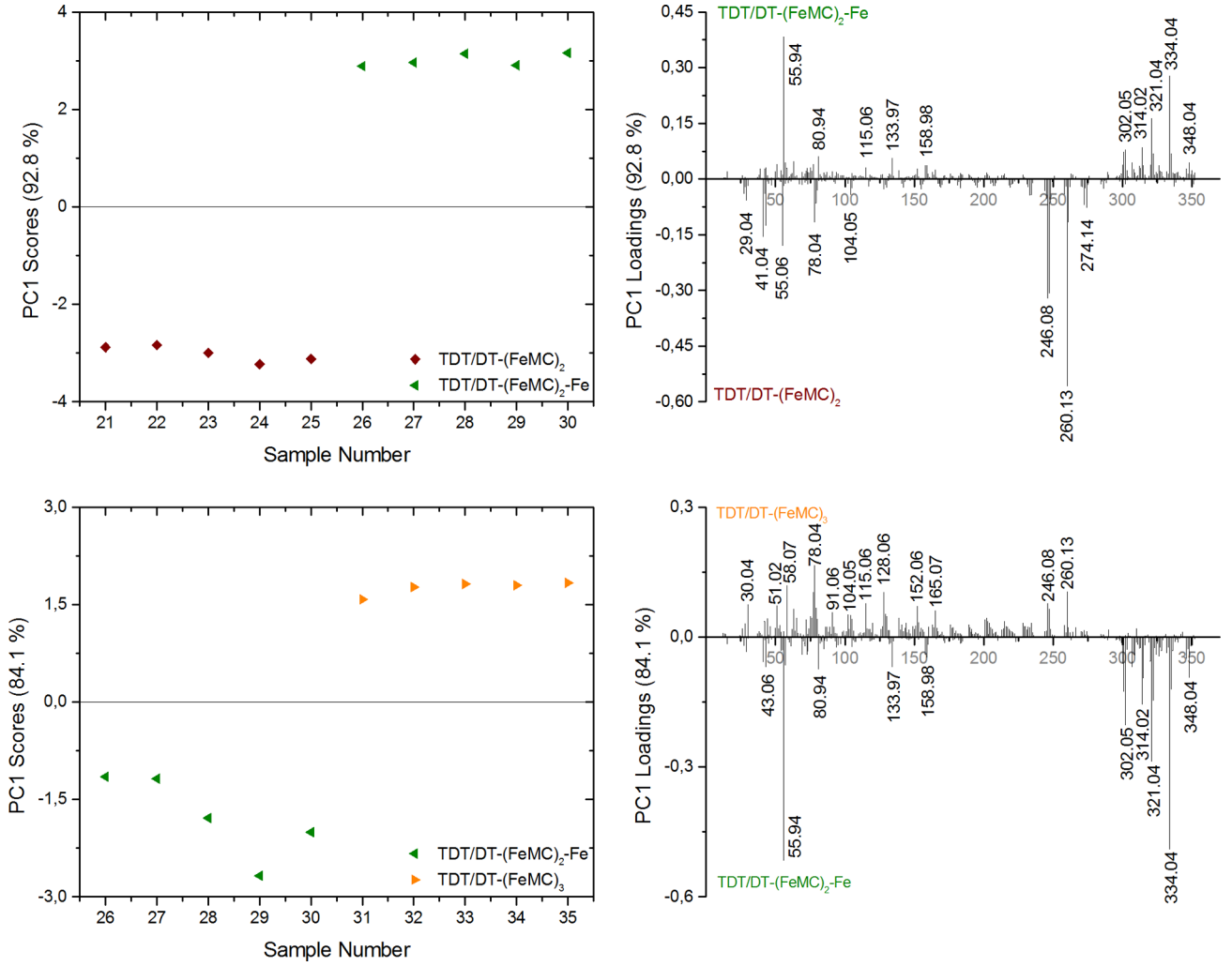

Figure 10. Scores and loadings plot for surface modification step 5 (top) and step 6 (bottom).

Table 2. Summary of the Highest Loading Peaks from the Positive-Ion Mode ToF-SIMS Spectra of the Layer-by-Layer (LbL) Self-Assembly[a]

m/z	assignment	*m/z*	assignment	*m/z*	assignment
29.04	$C_2H_5^+$	80.94	C_2HFe^+	247.12	$C_{16}H_{13}N_3^+$
30.04	CH_4N^+	91.06	$C_7H_7^+$	**260.13**	$C_{17}H_{14}N_3^+$
41.04	$C_3H_5^+$	**104.05**	$C_7H_6N^+$	**274.14**	$C_{18}H_{16}N_3^+$
43.06	$C_3H_7^+$	115.06	$C_9H_7^+$	289.03	$C_{15}H_{11}N_3Fe^+$
51.02	$C_4H_3^+$	128.05	$C_9H_6N^+$	302.04	$C_{16}H_{12}N_3Fe^+$
55.06	$C_4H_7^+$	133.97	$C_5H_4NFe^+$	309.04	$C_{15}H_{13}N_3Fe^+{\cdot}H_2O$
55.94	Fe^+	152.06	$C_{12}H_8^+$	314.03	$C_{17}H_{12}N_3Fe^+$
58.07	$C_3H_8N^+$	158.98	$C_7H_5NFe^+$	321.04	$C_{16}H_{13}N_3Fe^+{\cdot}H_2O$
73.05	$C_3H_7NO^+$	165.07	$C_{13}H_9^+$	334.05	$C_{17}H_{14}N_3Fe^+{\cdot}H_2O$
77.04	$C_6H_5^+$	**233.10**	$C_{15}H_{11}N_3^+$	348.05	$C_{18}H_{16}N_3Fe^+{\cdot}H_2O$
78.04	$C_5H_4N^+$	**246.08**	$C_{16}H_{12}N_3^+$		

[a]m/z values shown in boldface font are key fragments of the **MC**-terminated SAM highlighted by PCA.

evaporated. Therefore, assumption (ii) is the more-convincing conclusion.

A PCA was also carried out for the coordination step of Pd^{2+} to the PDS SAM (see scheme in Figure 1). Therefore, ~400 peaks were selected that could be assigned to the PDS and PDS + Pd SAM. Peaks unambiguously attributable to inorganic and PDMS contaminations were not included in this dataset. In principle, it would be sufficient to just check for the presence of Pd^+ secondary ions, which are, of course, detected at m/z = 105.90 with the typical isotope pattern, but a ToF-SIMS mass spectrum usually contains much more information. PCA, on one hand, helps to find this information and, on the other hand, helps to interpret it. Figure 6 shows the scores and the loadings plot of the surface modification with $Pd(CH_3CN)_4(BF_4)_2$. It can be clearly seen, in the positive loadings, that not only Pd^+ secondary ions are responsible for the separation of the two groups of samples,

dx.doi.org/10.1021/ac500059a | Anal. Chem. 2014, 86, 5740−5748

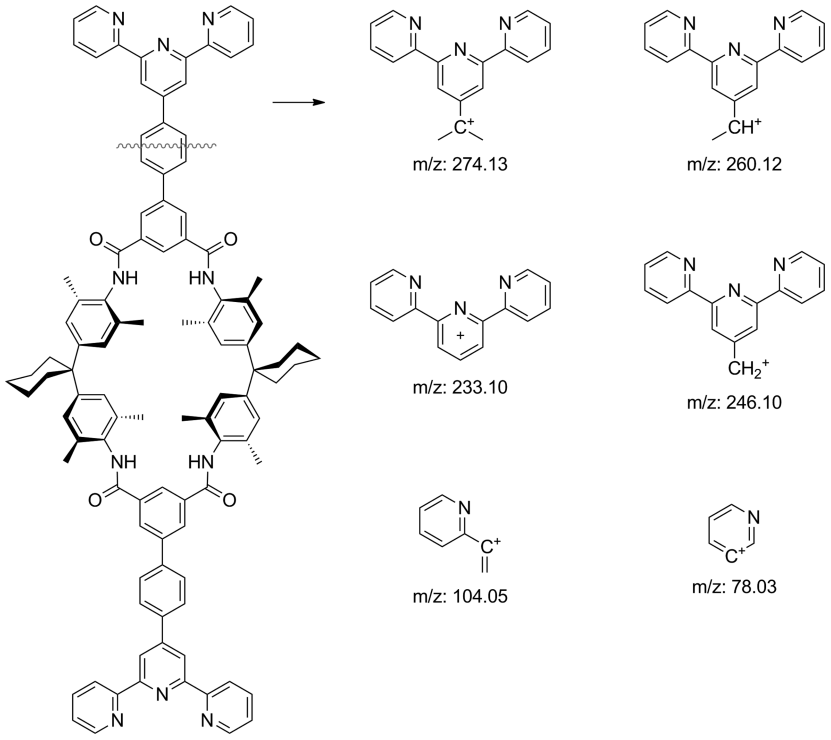

Figure 11. Structures of the main SIMS-fragments of the **MC**-terminated SAM highlighted by PCA. The wavy line shows where the main fragmentation takes place. The fragment ions depicted in the figure are not to be understood as sequential fragmentation. It is not clear whether this is a consecutive or a parallel fragmentation.

but also CH_2N^+ (a fragment ion from the neutral ligand CH_3CN) and adduct ions containing the CH_3CN ligand (e.g., $C_4H_5{\cdot}CH_3CN$, $Pd{\cdot}CH_3CN$) from the Pd precursor. The negative loadings are composed of secondary ions that can definitely be assigned to the PDS-SAM in Figure 3. Figure 6 not only shows that the coordination step was successful, but also that the surface composition is, as expected for the used Pd-precursor, composed of neutral CH_3CN ligands coordinated to Pd^{2+}. Another evidence for the coordination of Pd^{2+} to the surface ligand could be found due to the significant presence of F^- and BF_4^- secondary ions in the negative ion mode ToF-SIMS spectra.

Example 2: Layer-by-Layer Self-Assembly of Hunter/Vögtle-Type Tetralactam Macrocycles. To analyze the complex systems described in this example, each chemical surface modification step is monitored by ToF-SIMS.

The dataset consisted of spectra of five measurement spots per individual sample (see Table 1 for an overview of sample notation) with over 450 variables (i.e., peaks, m/z values). Known inorganic contaminants were not considered in the dataset.

Figure 7 shows scores plots of the entire dataset. Figure 7a shows that the individual samples are well-separated on PC1, although deviations in the mass spectra were not easily discernible by a univariate approach. The clustering of samples 6−10, 16−20, and 26−30 (Fe coordinated to the terpyridine end group) and samples 11−15 and 21−25 (terpyridine end group on the **MC**) on the nearly same PC1 score in the scores plot also indicates that these samples exhibit similar spectra. However, a plot of the PC1 scores versus the PC2 scores (Figure 7b) shows that only samples 11−15 and 21−25 and samples 16−20 and 26−30 cluster on similar coordinates. Samples 6−10 (**TDT**/**DT**-Fe), in contrast, are well-separated. Although samples 31−35 exhibit the same surface chemistry, i.e., the terpyridine end-group points toward the surface, a clustering similar to the other terpyridine-terminated **MC**s would have been expected. However, they are separated from them. The reason for this is unclear. It could be due to a change to a more-tilted orientation or due to an accumulation of defects in the course of stack formation.

To determine which variables (m/z values) are responsible for the separation in the scores plot for each chemical modification step, a PCA of the corresponding subsystems (e.g., **TDT**/**DT** and **TDT**/**DT**-Fe, **TDT**/**DT**-Fe and **TDT**/**DT**-Fe**MC**, etc.) was performed using always the same set of variables (i.e., peak list). Each PCA of the subsystem catches a huge amount of variance on PC1 (>94%, except for the last **MC** deposition step, which catches a variance of 84%), confirming an excellent separation of the samples. The resulting scores and the corresponding loadings plots showing the main variables of interest for each modification step are depicted in Figures 8, 9, and 10. The peaks with significant loadings are labeled with the measured mass and are summarized in Table 2. PC1 clearly discriminates the Fe-coordinated terpyridine group from the noncoordinated ones and the corresponding variables are highlighted in the loadings plot. The Fe coordinated end-group is reflected in the loadings plot where the loadings of the iron-containing secondary ions correlate with the corresponding Fe coordinated SAM. The PCA emphasizes not only the presence of Fe (main isotope at m/z = 55.94) as well as typical pyridine and terpyridine fragments coordinated with Fe (m/z = 133.97, 289.03, 302.04, 314.03), but also accentuates m/z values containing the neutral ligand H_2O to the Fe-coordinated terpyridine fragments (m/z = 309.04, 321.04, 334.05, 348.05). This clearly shows the presence of chemically bound water on the outermost surface originating from the used $Fe(BF_4)_2(H_2O)_6$ precursor. A ToF-SIMS

dx.doi.org/10.1021/ac500059a | *Anal. Chem.* 2014, 86, 5740−5748

spectrum acquired in negative-ion mode also shows the presence of BF_4^- secondary ions.

The **TDT**/**DT**-SAM, as well as the corresponding layers terminated with **MC**, are characterized by high loadings peaks containing pyridyl (m/z = 78.04) and terpyridyl (m/z = 247.12, 260.13, 274.14) fragment cations.

A recent MM2 force field modeling calculation shows that a densely packed macrocycle layer is tilted at an angle of 38° from the surface plane,[3] thus exposing the terpyridine end-group on top of the surface. This is also a possible explanation of the appearance of secondary ions highlighted by the PCA corresponding to this end group as listed in Table 2 (m/z values shown in boldface font) and shown in Figure 11, keeping in mind that the rest of the macrocycle is well-protected from impinging primary ions. The terpyridine group is cleaved from the macrocycle, as indicated by the gray wavy line in Figure 11. This fragment ion is subject to further fragmentation by losing C_xH_y, breaking the terpyridine, and finally leaving characteristic pyridine secondary ions. This is then further cleaved to unspecific hydrocarbons and N-containing hydrocarbons.

CONCLUSION

A time-of-flight secondary-ion mass spectrometry (ToF-SIMS) study supported by PCA was carried out on self-assembled monolayers, and a thin film system was grown by layer-by-layer (LbL) self-assembly, respectively. It was shown in example 1 how high-end surface analysis can help improve the quality of SAM formation. Different preparation procedures could be evaluated to select the best one for subsequent deposition steps. Example 2 showed how stepwise surface self-assembly can be monitored. Starting from a preordered SAM template, each step of the surface self-assembly was monitored by ToF-SIMS. With the use of PCA in this monitoring process, the quality of the layer stack could be controlled precisely. This is important for the bottom-up development of nanoscaled devices that may translate molecular stimuli into macroscopic effects.

The combination of both high-end surface analysis complemented and multivariate data analysis is a powerful tool for the development of high-quality layer stacks. PCA carves out differences between samples, i.e., even slight residues like sodium sulfate in example 1, a nonperfect self-assembly or marginal differences in signal intensity can be accentuated. Therefore, it is very important for the analyst to assess the trends seen in principal component analysis (PCA) and determine whether these trends are due to a mere artifact or due to real sample differences.

AUTHOR INFORMATION

Corresponding Author

*E-mail: markus.holzweber@bam.de.

Notes

The authors declare no competing financial interest.

ACKNOWLEDGMENTS

This research was supported by Deutsche Forschungsgemeinschaft (Grant Nos. SCHA893/9-1 and UN80/8-1). The authors thank Dan Graham (Molecular Engineering & Sciences Institute, University of Washington) for his advice in performing the PCA. M.H. is grateful for financial support by BAM through the Adolf−Martens fellowship program and by the Austrian Science Fund (FWF) through the Erwin−Schrödinger Fellowship Program (Project No. J 3471-N28).

REFERENCES

(1) Traulsen, C. H. H.; Kunz, V.; Heinrich, T.; Richter, S.; Holzweber, M.; Schulz, A.; von Krbek, L. K. S.; Poppenberg, J.; Scheuschner, U. T. J.; Unger, W. E. S.; Schalley, C. A. *Langmuir* **2013**, *29*, 14284−14292.
(2) Balzani, V.; Credi, A.; Raymo, F. M.; Stoddart, J. F. *Angew. Chem., Int. Ed.* **2000**, *39*, 3348−3391.
(3) Poppenberg, J.; Richter, S.; Traulsen, C. H. H.; Darlatt, E.; Baytekin, B.; Heinrich, T.; Deutinger, P. M.; Huth, K.; Unger, W. E. S.; Schalley, C. A. *Chem. Sci.* **2013**, *4*, 3131−3139.
(4) Richter, S.; Traulsen, C. H. H.; Heinrich, T.; Poppenberg, J.; Leppich, C.; Holzweber, M.; Unger, W. E. S.; Schalley, C. A. *J. Phys. Chem. C* **2013**, *117*, 18980−18985.
(5) Coskun, A.; Banaszak, M.; Astumian, R. D.; Stoddart, J. F.; Grzybowski, B. A. *Chem. Soc. Rev.* **2012**, *41*, 19−30.
(6) Benninghoven, A. *Angew. Chem., Int. Ed.* **1994**, *33*, 1023−1043.
(7) Richter, S.; Poppenberg, J.; Traulsen, C. H. H.; Darlatt, E.; Sokolowski, A.; Sattler, D.; Unger, W. E. S.; Schalley, C. A. *J. Am. Chem. Soc.* **2012**, *134*, 16289−16297.
(8) Traulsen, C. H. H.; Darlatt, E.; Richter, S.; Poppenberg, J.; Hoof, S.; Unger, W. E. S.; Schalley, C. A. *Langmuir* **2012**, *28*, 10755−10763.
(9) Poirier, G. E.; Pylant, E. D. *Science* **1996**, *272*, 1145−1148.
(10) Graham, D. J.; Castner, D. G. *Biointerphases* **2012**, *7*, 49.
(11) Muramoto, S.; Graham, D. J.; Wagner, M. S.; Lee, T. G.; Moon, D. W.; Castner, D. G. *J. Phys. Chem. C* **2011**, *115*, 24247−24255.
(12) Biesinger, M. C.; Paepegaey, P.-Y.; McIntyre, N. S.; Harbottle, R. R.; Petersen, N. O. *Anal. Chem.* **2002**, *74*, 5711−5716.
(13) Graham, D. J.; Ratner, B. D. *Langmuir* **2002**, *18*, 5861−5868.
(14) Wagner, M. S.; Castner, D. G. *Langmuir* **2001**, *17*, 4649−4660.
(15) Wagner, M. S.; Graham, D. J.; Ratner, B. D.; Castner, D. G. *Surf. Sci.* **2004**, *570*, 78−97.
(16) Poppenberg, J.; Richter, S.; Darlatt, E.; Traulsen, C. H. H.; Min, H.; Unger, W. E. S.; Schalley, C. A. *Surf. Sci.* **2012**, *606*, 367−377.
(17) Min, H.; Park, J.-W.; Shon, H. K.; Moon, D. W.; Lee, T. G. *Appl. Surf. Sci.* **2008**, *255*, 1025−1028.